

Motion and Torque Analyses of Swiss Lever Escapement Mechanism for Energy Harvesting Application

Feng-Ming Ou* and Hsu-Chien Wu

Department of Mechanical Engineering, National Cheng Kung University,
No. 1, University Road, Tainan City 70101, Taiwan

(Received January 10, 2025; accepted April 23, 2025)

Keywords: Swiss lever escapement mechanism, piezoelectric energy harvesting, motion and torque analyses, excitation strategy, power density

Piezoelectric energy harvesting (PEH) leverages the piezoelectric effect to convert mechanical strain into electrical energy. Its high output voltage, low output current, and potential for miniaturization make it an attractive solution to powering micropower generation sensors and devices. In this study, we investigate the integration of the Swiss lever escapement mechanism with PEH to improve energy conversion efficiency under low-frequency conditions. On the basis of motion and torque analyses of escapement mechanisms, strategies were developed for optimal excitation state and design parameters, including hairspring stiffness, applied torque, and moment of inertia, which were identified as the critical factors affecting torque variations. COMSOL Multiphysics® simulations demonstrated that the proposed system achieves stable power outputs of 86.8, 15.3, and 0.27 μW when the balance wheel, escape wheel, and pallet fork were used as excitation sources, respectively. Furthermore, the average power density of 2.245 $\mu\text{W}/\text{cm}^3$ obtained by the balance wheel excitation under the optimal state shows considerable opportunity and potential for practical applications. This work provides a foundation for the further optimization of escapement mechanisms and piezoelectric energy harvesters to enhance sustainability and performance.

1. Introduction

With the rapid advancement of technology, energy consumption and environmental pollution have significantly increased, emphasizing the urgent need for sustainable energy solutions. Among various strategies, energy harvesting has emerged as a promising field, focusing on converting energy from environmental sources such as solar, thermal, wind, and vibrational energy into electrical power. Different energy harvesting techniques, including triboelectric,⁽¹⁾ electrostatic,⁽²⁾ electromagnetic,⁽³⁾ and piezoelectric methods,⁽⁴⁾ offer distinct advantages depending on application scenarios.

Piezoelectric energy harvesting (PEH) leverages the piezoelectric effect to convert mechanical strain into electrical energy. Its high output voltage, low output current, and potential

*Corresponding author: e-mail: ou_fm@gs.ncku.edu.tw
<https://doi.org/10.18494/SAM5541>

for miniaturization make it an attractive solution to powering micropower generation sensors and devices.⁽⁵⁾ However, the low-frequency nature of ambient vibrations limits PEH efficiency.⁽⁶⁾ Researchers have proposed methods such as bandwidth enhancement^(7–9) and frequency-up conversion^(10,11) to address these limitations, enabling the conversion of random, low-frequency vibrations into higher and more stable frequencies.

To further improve energy harvesting efficiency, some studies have proven the potential of integrating the escapement mechanism into energy harvesting systems. The mechanism regulates the release of stored energy in a controlled manner, transforming irregular motion into a more uniform excitation source. Such energy harvesting systems are particularly suitable for monitoring infrastructure (e.g., bridges, railways), industrial machinery, and vibration-powered IoT nodes, where space is sufficient, motion is repetitive or stochastic, and battery replacement is impractical. By enabling frequency regulation and impulse-based excitation, escapement-assisted PEH systems can enhance stability and power density under low-frequency, nonuniform excitation conditions. Recent studies have applied escapement mechanisms to triboelectric nanogenerators (TENGs)^(12–15) and PEH.⁽¹⁶⁾ Taking PEH as an example, Zhang *et al.*⁽¹⁶⁾ utilized a frequency regulator to achieve a stable power output from a piezoelectric cantilever beam at an excitation frequency of 1 Hz, generating an average power of 10.03 μW with a power density of 0.324 $\mu\text{W}/\text{cm}^3$. However, none of these studies addressed the design or excitation strategy of escapement mechanisms.

Therefore, we investigated how various parameters of the escapement mechanism affect the energy conversion efficiency of a piezoelectric cantilever beam. By leveraging the proportional relationship between excitation force and power generation,^(17,18) we focused on three objectives: (1) identifying the optimal component of the escapement mechanism to serve as the excitation source, (2) determining the motion state that maximizes excitation timing of the piezoelectric beam, and (3) analyzing critical design parameters to enhance performance. A case study is provided to demonstrate the energy harvesting and power generation capabilities by the proposed approach.

2. Parameters and Dynamic Modeling of Escapement Mechanism

The escapement mechanism, commonly used in clocks and watches, is responsible for regulating timekeeping by converting irregular motion into periodic motion.⁽¹⁹⁾ The Swiss lever escapement shown in Fig. 1, known for its high accuracy and reliability, is widely adopted in timepieces. Its components include an escape wheel, a pallet fork, a balance wheel, a hairspring, and two banking pins. Torque applied to the escape wheel drives its rotation, while the elasticity of the hairspring provides a restoring force that enables the balance wheel to oscillate. The pallet fork regularly releases and stops the escape wheel through the movement of the balance wheel, and the banking pins are used to limit the position of the pallet fork.

The mechanism operates in four primary phases during a half cycle: locking, unlocking, impulse, and safety. These phases encompass seven impact periods ($P_1, P_{1p}, P_2, P_3, P_4, P_5,$ and P_6), forming a complete motion cycle after two half cycles. Figure 2 illustrates these states, highlighting the periodic transitions between motion phases.

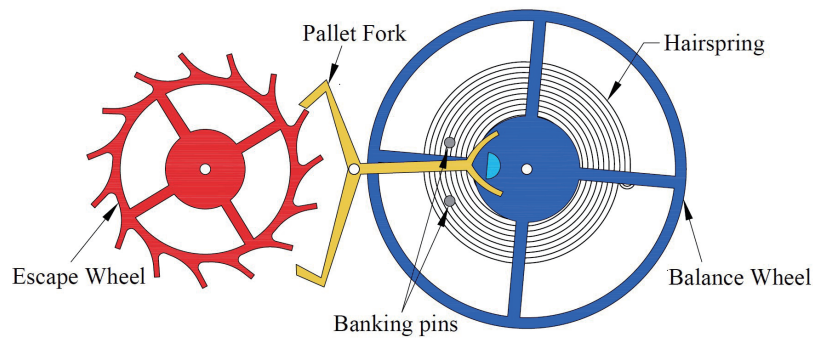


Fig. 1. (Color online) Swiss lever escapement mechanism.

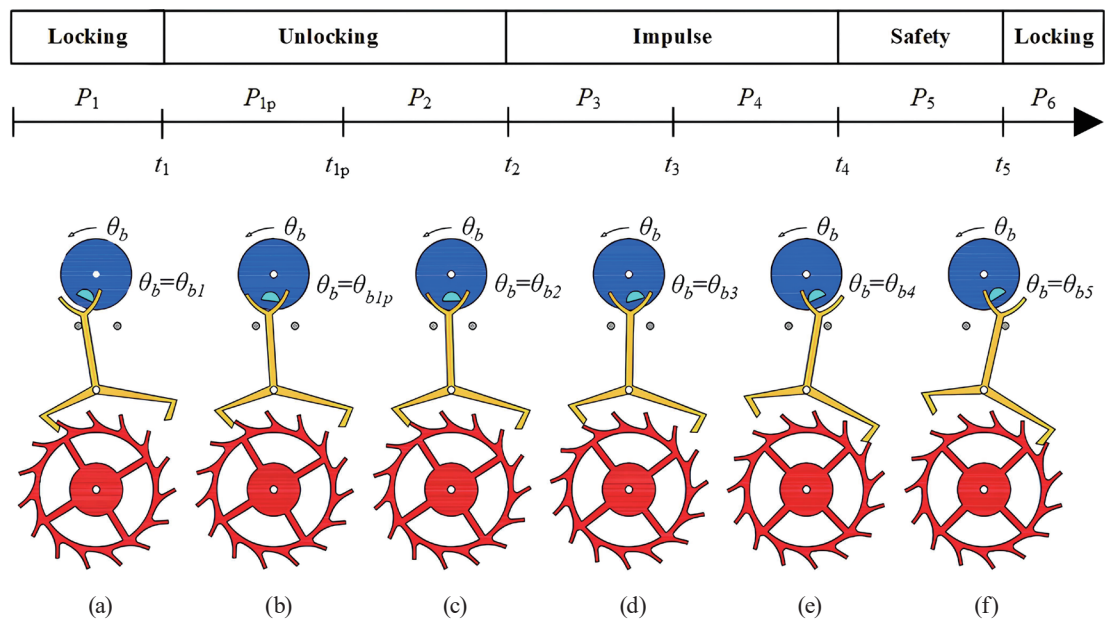


Fig. 2. (Color online) Motion states in a half cycle of the Swiss lever escapement mechanism. (a) $t = t_1$, (b) $t = t_{1p}$, (c) $t = t_2$, (d) $t = t_3$, (e) $t = t_4$, and (f) $t = t_5$.

To apply the escapement mechanism to piezoelectric energy harvesting, Three excitation scenarios involving the balance wheel, pallet fork, and escape wheel are presented in Fig. 3. In each scenario, mechanical energy is transferred through impulse or contact force, inducing strain in the piezoelectric cantilever beam, which is then converted into electrical energy through the piezoelectric effect. In this study, the parameters and torque characteristics of each component are systematically investigated under different motion states to evaluate their effectiveness for energy harvesting applications.

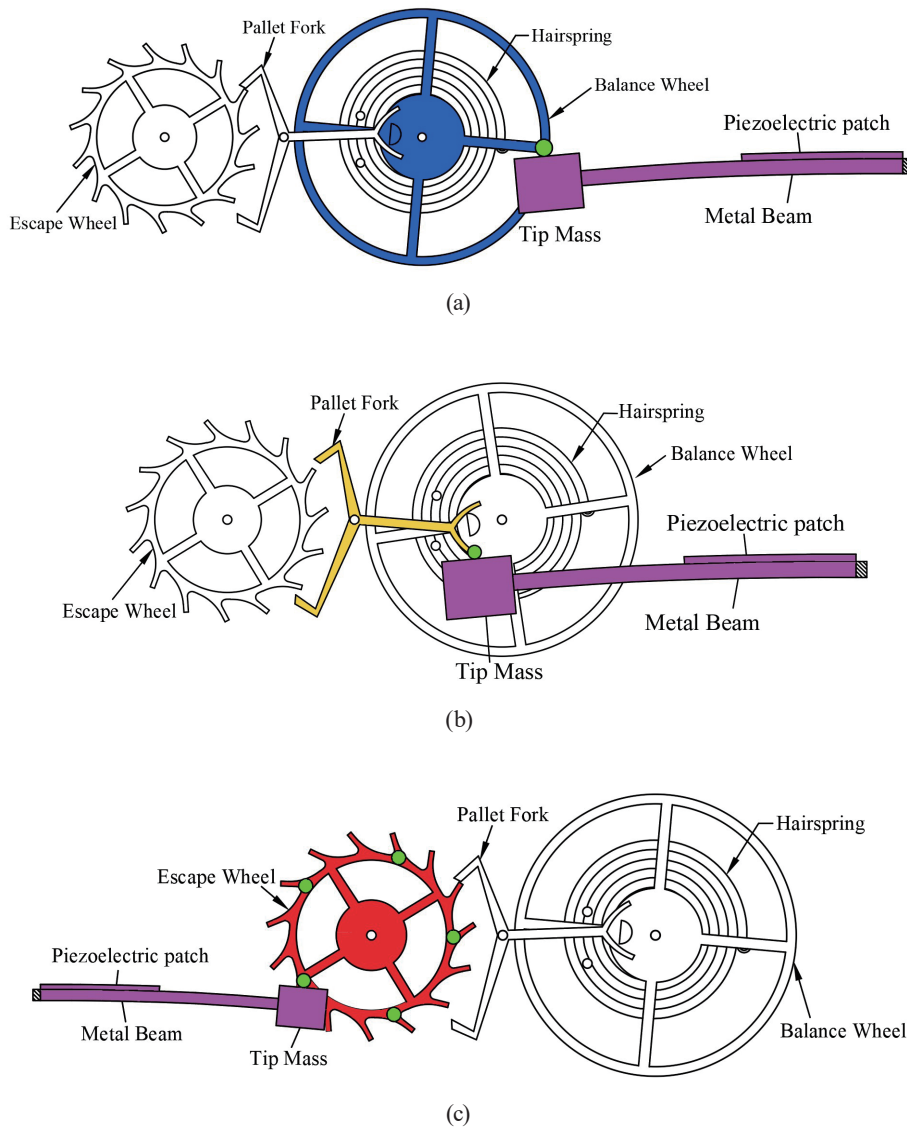


Fig. 3. (Color online) Three excitation scenarios for the piezoelectric cantilever beam: (a) balance wheel, (b) pallet fork, and (c) escape wheel.

2.1 Key parameters and constraints

Table 1 and Fig. 4 show definitions of the mechanism parameters, including distances, radii, moments of inertia, stiffness, friction coefficients, and torque. Owing to the asymmetric design of the pallet fork, two sets of geometric parameters are required for comprehensive modeling. Some constraints are necessary to ensure operational effectiveness, for instance, the distance D_1 between the escape wheel and pallet fork must exceed specific radii R_E , R_{P1} , and R_{P2} , and the distance D_2 between the pallet fork and the balance wheel must be greater than the radius of the balance wheel. These constraints are vital for preserving the mechanism's functionality and precision.

Table 1
Definitions and constraints of mechanism parameters.

Independent Parameter	Definition	Dependent Parameter	Constraints
D_1	Distance between the escape wheel and the pallet fork	$R_1, R_2, R_5, R_6,$	$R_E < D_1$
R_E	Radius of the escape wheel	R_7, R_9, L_1, L_2	$R_{P1_En} < D_1$
R_{P1_En}	Radius of the entry pallet fork during unlocking phase	$R_5, R_6, R_7, L_1,$	$R_{P2_En} < D_1$
R_{P2_En}	Radius of the entry pallet fork during impulse phase	L_2	$R_{P1_Ex} < R_E$
R_{P1_Ex}	Radius of the exit pallet fork during unlocking phase	$R_1, R_2, R_9, L_1,$	$R_{P2_Ex} < R_E$
R_{P2_Ex}	Radius of the exit pallet fork during impulse phase	L_2	$R_{P2} < R_{P1}$
D_2	Distance between the pallet fork and the balance wheel	R_3, R_4, L_3, L_4	$R_B < D_2$
R_B	Radius of the impulse pin of the balance wheel		
J_P	Moment inertia of the pallet fork	–	
J_E	Moment inertia of the escape wheel	–	
K	Stiffness of the hairspring	J_B	
μ	Friction coefficient between escape wheel and pallet fork	–	< 0.5
τ_E	Torque exerted on the escape wheel	–	

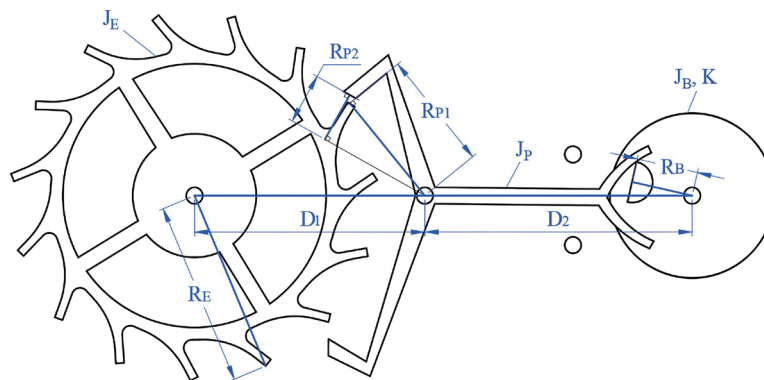


Fig. 4. (Color online) Key parameters in the Swiss lever escapement mechanism.

2.2 Dynamic modeling

The escapement mechanism's motion can be modeled as a periodically forced oscillation with impacts. Nonlinear dynamic behavior⁽²⁰⁾ is analyzed using impulse differential equations⁽²¹⁾ to determine the displacement, velocity, and acceleration of its components (escape wheel, pallet fork, and balance wheel). Equation (1) defines the system's state transitions during impact events, where t_k denotes the instant of impact, $x(t)$ represents the state vector, $f(t, x(t))$ is the dynamic equation of the system, $\rho(x(t_k^-))$ indicates the jump variable at the moment of impact, and $x(t_k^-)$ represents the state of the system just prior to the moment of impact. Equation (2) is the governing equation of the escapement mechanism at state P_1 , where x is defined as the initial angles and velocities; thus, the angular velocities and accelerations at the moment of impact can be obtained by calculation using the equation. The Euler method is applied to update x after a time interval of Δt , which will serve as the initial condition for subsequent calculations. Additional relevant equations can be found in Ref. 19.

$$\begin{cases} \dot{x} = f(t, x(t)), t \neq t_k \\ \Delta x|_{t=t_k} = \rho(x(t_k^-)), k \in N \end{cases} \quad (1)$$

$$\dot{x} = \begin{bmatrix} -K/J_B & 0 & 0 \\ 0 & 0 & 0 \\ 0 & 0 & 0 \end{bmatrix} x, x \in P_1 \text{ and } x \equiv [\theta_B, \theta_P, \theta_E, \dot{\theta}_B, \dot{\theta}_P, \dot{\theta}_E]^T \quad (2)$$

Accordingly, torque variations across components are computed using Eq. (3), enabling comprehensive parameter analyses and the development of an effective excitation strategy.

$$\tau = J \cdot \ddot{\theta} \quad (3)$$

3. Excitation Strategy

The escapement mechanism serves as the excitation system for the piezoelectric cantilever beam, with the excitation force directly affecting power generation. In this section, we examine the conditions under which maximum torque occurs within the escapement mechanism and evaluate how design parameters impact torque, providing critical insights for energy harvesting application.

3.1 Identification of key excitation states

On the basis of the parameters outlined in Sect. 2.1, 13 independent variables were identified. In this study, we employed the Taguchi method for parameter analyses, utilizing an L_{27} orthogonal array comprising 13 factors at three levels with the corresponding values estimated from an existing design, as presented in Table 2. Through the governing equations of the escapement mechanism described in Sect. 2.2, the angular positions, velocities, accelerations, as well as torque values for the balance wheel, pallet fork, and escape wheel of the 27 combinations were computed across 14 states of two half cycles.

Figure 5 shows the proportion of occurrences of the two largest average torques generated by the balance wheel, pallet fork, and escape wheel at each state. The balance wheel, pallet fork, and escape wheel exhibit the highest proportion of larger torque generation during state P_3 in the 2nd half of the cycle. For the balance wheel, the next highest torque generation occurs during state P_3

Table 2
Thirteen factors and three levels for parameter analyses.

Factor	D_1 (mm)	D_2 (mm)	R_B (mm)	R_E (mm)	R_{P1_En} (mm)	R_{P2_En} (mm)	R_{P1_Ex} (mm)	R_{P2_Ex} (mm)	J_P (kgm ²)	J_E (kgm ²)	K (Nm/ rad)	μ	τ_E (Nm)
Level 1	27.9	36.9	7.74	20.55	13.87	7.63	22.59	11.6	0.99e-4	1.98e-4	3.06e-3	0.207	0.9e-2
Level 2	28	37	7.84	20.65	13.97	7.73	22.69	11.7	1.10e-4	2.20e-4	3.40e-3	0.230	1.0e-2
Level 3	28.1	37.1	7.94	20.75	14.07	7.83	22.79	11.8	1.20e-4	2.42e-4	3.74e-3	0.253	1.1e-2

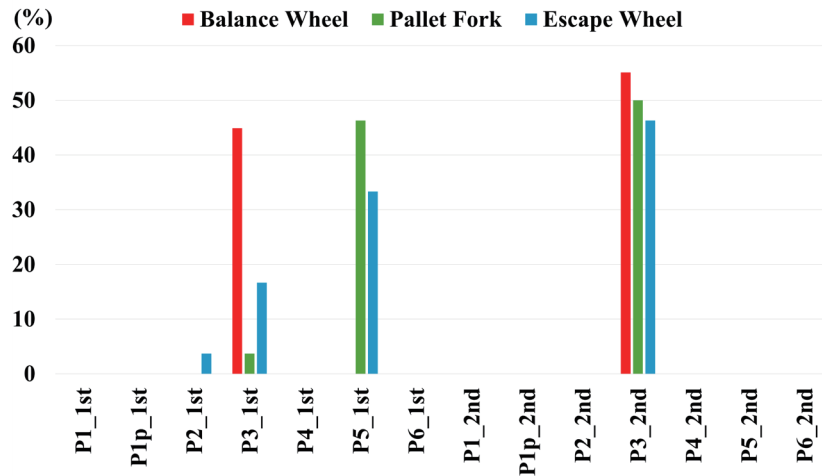


Fig. 5. (Color online) Proportion charts of state for the top two highest torques during a cycle.

in the 1st half of the cycle, whereas for the pallet fork and escape wheel, it occurs during state P_5 in the 1st half of the cycle.

3.2 Key parameters affecting torque performance

Furthermore, the impact of various parameters on torque was analyzed across 14 states of the escapement mechanism. Results showed that the stiffness K of hairspring is the most significant factor affecting the variation of the balance wheel torque. In most states, the impact of K surpasses that of other factors, particularly in states P_1 , P_4 , and P_5 . However, in states P_{1p} , P_2 , P_3 , and P_6 , factors τ_E and J_E also exert a noticeable effect on the torque. For the pallet fork, no torque is generated in the P_1 and P_6 states, making it impossible to observe the effect of any factor. The remaining states, J_p , K , and τ_E , are dominant factors that consistently rank among the top three most influential factors, with their rankings differing across various states. The analysis of the situation regarding the escape wheel reveals that the states P_1 and P_6 are identical to those of the pallet fork, making it impossible to determine the influential factors. Among the rest states, τ_E is consistently the most significant factor, particularly in P_2 , P_4 , and P_5 , and followed by the parameters K and J_E .

To summarize, stiffness K is the most critical factor affecting torque variations in the balance wheel, with torque τ_E and the moment of inertia J_E also playing significant roles. For the pallet fork, the key influential factors are J_p , K , and τ_E . In the case of the escape wheel, the torque τ_E is the dominant parameter, followed by the stiffness K and the moment of inertia J_E .

4. Case Study

A simulation study was conducted to evaluate the performance of the piezoelectric cantilever beam activated by the escapement mechanism. On the basis of the analyses and findings

described in Sect. 3, a specific parameter set for the escapement mechanism was established. The motion frequency was set to 1 Hz, consistent with the proposed excitation strategy, to validate its effectiveness.

4.1 System configuration

On the basis of the construction and the natural frequency⁽²²⁾ for the piezoelectric beam, as illustrated in Fig. 6 and described in Eq. (4), an appropriate set of parameters for the PEH is established in Table 3, with a target natural frequency $f_n = 30$ Hz.

$$f_n = \frac{1}{2\pi} \sqrt{\frac{\frac{3E_b I_b}{L_b^3} + \frac{3E_p I_p}{L_p^3}}{\frac{33}{140}(m_b + m_p) + m_a}} \tag{4}$$

In terms of the escapement mechanism, the torque variation of the balance wheel, pallet fork, and escape wheel over one complete cycle (comprising two half cycles) can be calculated using the dynamic model outlined in Sect. 2.2. The results are presented in Fig. 7, where the colors red, orange, yellow, green, blue, dark blue, and purple represent the states $P_1, P_{1p}, P_2, P_3, P_4, P_5,$ and P_6 , respectively. It is clear that the highest torques for the balance wheel, pallet fork, and escape

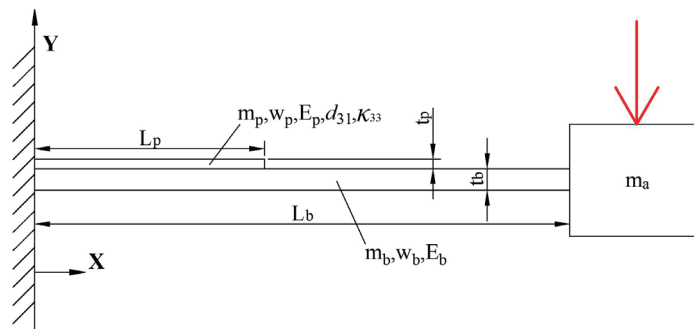


Fig. 6. (Color online) Diagram of piezoelectric cantilever beam.

Table 3
Parameters of piezoelectric cantilever beam.

Parameter	Unit	Beam (b)	MFC-2807P2 (p)
Length (L)	mm	65	28
Width (w)	mm	7	7
Thickness (t)	mm	0.3	0.3
Young's Modulus (E)	GPa	101.74	15.857
Mass (m)	g	1.606	0.32
d_{31}	pC/N	–	–210
κ_{33}	nF/m	–	19.7

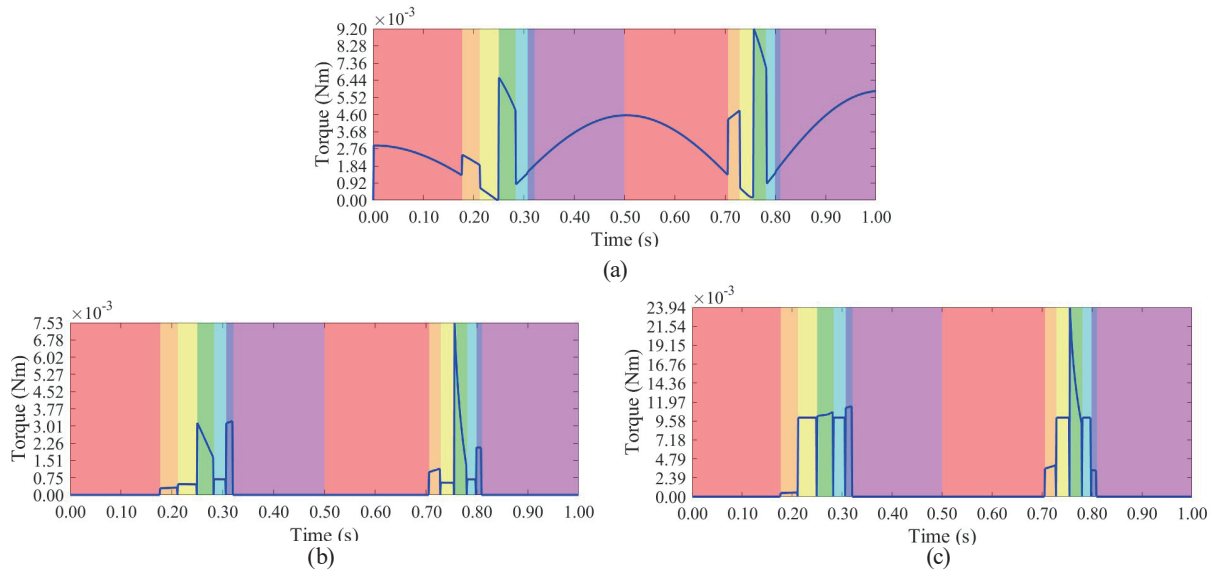


Fig. 7. (Color online) Torque variation over one cycle: (a) balance wheel, (b) pallet fork, and (c) escape wheel.

wheel occur during the P_3 state in the 2nd half cycles, which aligns with the key excitation state identified in Fig. 5.

4.2 Simulation results

According to Eq. (4) and the parameters defined in Table 3, the piezoelectric beam model was constructed and simulated using COMSOL Multiphysics[®] software. The excitation source was selected individually from the balance wheel, pallet fork, and escape wheel, each equivalently modeled as an impulse generator with a duration of 0.01 s. The excitation timing was applied at state P_3 of the 2nd cycle for all three components, as shown in Fig. 7. The corresponding simulation results are summarized as follows.

- *Balance wheel*: The average torque in state P_3 of the 2nd cycle is 7.00×10^{-3} Nm, corresponding to the excitation force of 0.9044 N when divided by R_B . As shown in Fig. 8(a), this configuration generates the highest average electric energy, 1.3 mJ over 30 s, equating to an electric power of 86.8 μ W.
- *Pallet fork*: The average torque in the same state is 3.24×10^{-3} Nm, translating to the excitation force of 0.1422 N when divided by R_{P1_Ex} . As shown in Fig. 8(b), this setup generates the lowest electric energy, 8.01 μ J, or 0.27 μ W.
- *Escape wheel*: The average torque in state P_3 of the 2nd cycle is 1.2×10^{-2} Nm, resulting in an excitation force of 0.5811 N when divided by R_E . As shown in Fig. 8(c), this scenario produces an average electric energy of 0.46 mJ, corresponding to 15.3 μ W.

The simulation results showed that the balance wheel provided the largest excitation force and the highest power output, followed by the escape wheel and pallet fork. Smaller excitation forces required longer periods for voltage stabilization, demonstrating the importance of selecting optimal excitation components and states to maximize energy harvesting efficiency.

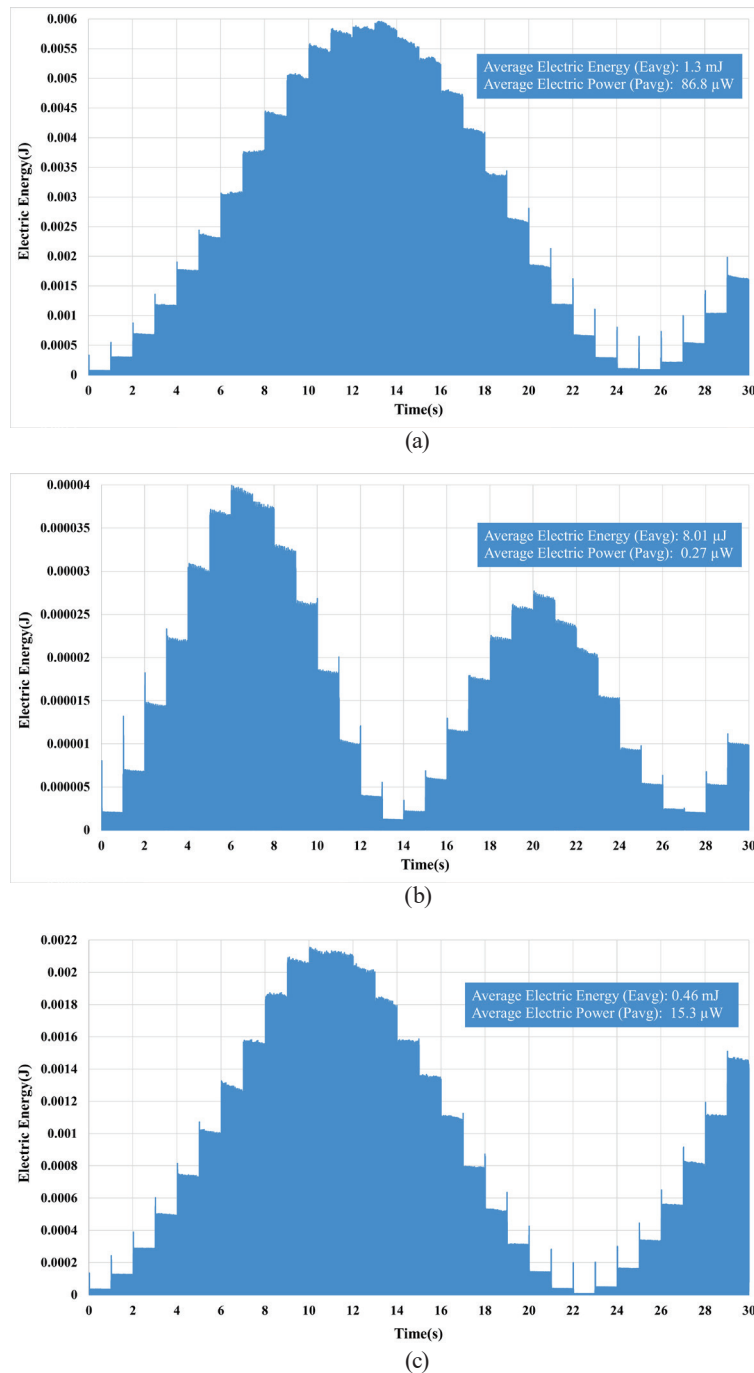


Fig. 8. (Color online) Electric energy charts for the excitation by different components: (a) balance wheel excitation, (b) pallet fork excitation, and (c) escape wheel excitation.

Further comparison of the result with a previous related study,⁽¹⁶⁾ which revealed an average power density of 0.324 μ W/cm³, showed that the proposed approach demonstrates a significant improvement, achieving a power density of 2.245 μ W/cm³. This highlights the great potential of the proposed strategy for practical validation and implementation.

5. Conclusions

In this study, we explored the integration of the Swiss lever escapement mechanism with piezoelectric energy harvesters, offering strategies to optimize design parameters for improving energy conversion efficiency. The primary conclusions are as follows:

- 1) The balance wheel generates the highest average torque in state P_3 , making it the most suitable excitation source for the piezoelectric cantilever beam.
- 2) Key parameters, including stiffness (K), torque (τ_E), and moment of inertia, are identified as critical factors affecting torque variations across the escapement mechanism.
- 3) Simulation results showed stable power outputs under harmonic resonance conditions: 86.8 μW for the balance wheel, 15.3 μW for the escape wheel, and 0.27 μW for the pallet fork as excitation sources.
- 4) The simulation of the proposed system demonstrates higher potential in average power and power density compared with a previous study⁽¹⁶⁾ under low-frequency excitation conditions.

These findings provide valuable insights for the advancement of escapement-piezoelectric energy harvesting systems. In future research, we can further explore the optimization of excitation components and escapement mechanism designs under various operational conditions, ensuring maximum torque and energy efficiency through parameterized design approaches.

Acknowledgments

The authors are grateful to the National Science and Technology Council, Taiwan, R.O.C. for the financial support of this research under grant number NSTC 112-2222-E-006-003-MY2.

References

- 1 J. Chen, and Z. L. Wang: *Joule* **1** (2017) 480. <https://doi.org/10.1016/j.joule.2017.09.004>
- 2 S. Meninger, J. O. Mur-Miranda, R. Amirtharajah, A. P. Chandrakasan, and J. H. Lang: *IEEE Trans. Very Large-Scale Integr. (VLSI) Syst.* **9** (2001) 64. <https://doi.org/10.1109/92.920820>
- 3 G. Miao, S. Fang, S. Wang, and S. Zhou: *Appl. Energy* **305** (2022) 117838. <https://doi.org/10.1016/j.apenergy.2021.117838>
- 4 A. Ali, S. Iqbal, and X. Chen: *Energy Strategy Rev.* **53** (2024) 101422. <https://doi.org/10.1016/j.esr.2024.101422>
- 5 N. Sezer and M. Koç: *Nano Energy* **80** (2021) 105567. <https://doi.org/10.1016/j.nanoen.2020.105567>
- 6 R. Ahmed, F. Mir, and S. Banerjee: *Smart Mater. Struct.* **26** (2017) 085031. <https://doi.org/10.1088/1361-665X/aa7bfb>
- 7 I. Sari, T. Balkan, and H. Kulah: *Sens. Actuators, A* **145-146** (2008) 405. <https://doi.org/10.1016/j.sna.2007.11.021>
- 8 M. Fang, Q. Liao, J. Wang, L. Qin, C. Zhong, and D. Zhang: *Int. J. Appl. Ceram. Technol.* **15** (2018) 1268. <https://doi.org/10.1111/ijac.12886>
- 9 S. E. Chen, W. Y. Chen, R. Y. Yang, and C. C. Wu: *Energy Convers. Manage. X* **20** (2023) 100463. <https://doi.org/10.1016/j.ecmx.2023.100463>
- 10 S. Wei, H. Hu, and S. He: *Smart Mater. Struct.* **22** (2013) 105020. <https://doi.org/10.1088/0964-1726/22/10/105020>
- 11 Y. Wu, J. Qiu, F. Kojima, W. Xie, and S. Zhou.: *AIP Adv.* **9** (2019) 045312. <https://doi.org/10.1063/1.5093361>
- 12 G. He, Y. Luo, Y. Zhai, Y. Wu, J. You, R. Lu, S. Zeng, and Z. L. Wang: *Nano Energy* **87** (2021) 106195. <https://doi.org/10.1016/j.nanoen.2021.106195>
- 13 K. D. Pham, D. Bhatia, N. D. Huynh, H. Kim, J. M. Baik, Z. H. Lin, and D. Choi: *Nano Energy* **89** (2021) 106350. <https://doi.org/10.1016/j.nanoen.2021.106350>

- 14 K. W. Han, J. N. Kim, A. Rajabi-Abhari, V. T. Bui, J. S. Kim, D. Choi, and I. K. Oh: *Adv. Energy Mater.* **11** (2021) 2002929. <https://doi.org/10.1002/aenm.202002929>
- 15 H. Li, Y. Zhang, Z. Gao, L. Liang, X. Wang, X. Liu, Y. Wu, and H. Zheng: *Nano Energy* **109** (2023) 108266. <https://doi.org/10.1016/j.nanoen.2023.108266>
- 16 Q. Zhang, Z. Liu, X. Jiang, Y. Peng, C. Zhu, and Z. Li: *Sustainable Energy Technol. Assess.* **53** (2022) 102591. <https://doi.org/10.1016/j.seta.2022.102591>
- 17 R. C. Hibbeler: *Mechanics and Materials*. (Pearson Education. Inc, London, 2018) 10th ed.
- 18 N. Jalili: *Piezoelectric-Based Vibration Control*. (Springer, New York, 2010).
- 19 R. Du and L. Xie: *The Mechanics of Mechanical Watches and Clocks*. (Springer, Berlin, 2012) Chap. 3.
- 20 J. Mao, Y. Fu, and P. Li: *Shock and Vib.* **20** (2013) 1001. <https://doi.org/10.3233/SAV-130800>
- 21 M. Perestyuk: *Impulsive Differential Equation*. Institute of Mathematics, Academy of Science of the Czech Republic (2011)
- 22 S. S. Rao: *Mechanical Vibrations*. (Prentice Hall, New Jersey, 2011) 5th ed.

About the Authors



Feng-Ming Ou received his M.S. and Ph.D. degrees from the Department of Mechanical Engineering, National Cheng Kung University (NCKU), Taiwan, in 2000 and 2005, respectively. He was a researcher at the Industrial Technology Research Institute from 2005 to 2011 and was the head of a modernization department in the footwear industry from 2011 to 2022. Since 2022, he has been an assistant professor at NCKU. His research interests are in mechanism and machine design, energy harvesting, and industrial automation and digitalization. (ou_fm@gs.ncku.edu.tw)



Hsu-Chien Wu received her B.E. degree from the Department of Mechanical Engineering, National Cheng Kung University (NCKU), Taiwan, in 2023. She is currently a graduate student at NCKU. Her research interests are in mechanism design and piezoelectric energy harvesting. (N16124759@gs.ncku.edu.tw)